ZR | Zoological Research

Article   **Open Access**

PCDH17 restricts dendritic spine morphogenesis by regulating ROCK2-dependent control of the actin cytoskeleton, modulating emotional behavior

Laidong Yu[1,2,#], Fangfang Zeng[1,2,#], Mengshu Fan[1,2], Kexuan Zhang[1,2], Jingjing Duan[1,3,4], Yalu Tan[1,3,4], Panlin Liao[1,3,4], Jin Wen[1,2], Chenyu Wang[1], Meilin Wang[1], Jialong Yuan[1,2], Xinxin Pang[1,2], Yan Huang[1,3,4], Yangzhou Zhang[1,3,4], Jia-Da Li[2,5,6,*], Zhuohua Zhang[1,2,6,7,*], Zhonghua Hu[1,2,3,4,6,*]

[1] *Hunan Key Laboratory of Molecular Precision Medicine, Department of Critical Care Medicine, Xiangya Hospital, Central South University, Changsha, Hunan 410008, China*

[2] *Center for Medical Genetics and Hunan Key Laboratory of Medical Genetics, School of Life Sciences, Central South University, Changsha, Hunan 410008, China*

[3] *National Clinical Research Center for Geriatric Disorders, Xiangya Hospital, Central South University, Changsha, Hunan 410008, China*

[4] *Hunan Provincial Clinical Research Center for Critical Care Medicine, Xiangya Hospital, Central South University, Changsha, Hunan 410008, China*

[5] *Hunan Key Laboratory of Animal Models for Human Diseases, School of Life Sciences, Central South University, Changsha, Hunan 410008, China*

[6] *MOE Key Lab of Rare Pediatric Diseases, School of Life Sciences, Central South University, Changsha, Hunan 410008, China*

[7] *Department of Neurosciences, University of South China Medical School, Hengyang, Hunan 421001, China*

ABSTRACT

Proper regulation of synapse formation and elimination is critical for establishing mature neuronal circuits and maintaining brain function. Synaptic abnormalities, such as defects in the density and morphology of postsynaptic dendritic spines, underlie the pathology of various neuropsychiatric disorders. Protocadherin 17 (PCDH17) is associated with major mood disorders, including bipolar disorder and depression. However, the molecular mechanisms by which PCDH17 regulates spine number, morphology, and behavior remain elusive. In this study, we found that PCDH17 functions at postsynaptic sites, restricting the number and size of dendritic spines in excitatory neurons. Selective overexpression of PCDH17 in the ventral hippocampal CA1 results in spine loss and anxiety- and depression-like behaviors in mice. Mechanistically, PCDH17 interacts with actin-relevant proteins and regulates actin filament (F-actin) organization. Specifically, PCDH17 binds to ROCK2, increasing its expression and subsequently enhancing the activity of downstream targets such as LIMK1 and the phosphorylation of cofilin serine-3 (Ser3). Inhibition of ROCK2 activity with belumosudil (KD025) ameliorates the defective F-actin organization and spine structure induced by PCDH17 overexpression, suggesting that ROCK2 mediates the effects of PCDH17 on F-actin content and spine development. Hence, these findings reveal a novel mechanism by which PCDH17 regulates synapse development and behavior, providing pathological insights into the neurobiological basis of mood disorders.

INTRODUCTION

Synapses are specialized contact sites that mediate information transfer from a presynaptic neuron to a postsynaptic cell (Südhof, 2018). The morphogenesis and plasticity of synapses are essential for the establishment, maturation, and remodeling of neuronal circuit connectivity,

underlying behavioral activities such as mood and memory. Most excitatory synapses occur at dendritic spines, tiny protrusions extending from dendrites (Berry & Nedivi, 2017). Alterations in the number and morphology of dendritic spines occur during development and in response to experience and environmental exposure (Alvarez & Sabatini, 2007; Penzes et al., 2011). Defects in the formation, elimination, and remodeling of dendritic spines are widely recognized as critical pathological mechanisms underpinning many neuropsychiatric diseases, including schizophrenia, bipolar disorder, and depression (Forrest et al., 2018; Penzes et al., 2011).

The establishment of dendritic spines depends on the coordination of complex molecular machinery located at the synapses (Tada & Sheng, 2006). A vast array of synaptic proteins, many encoded by genes associated with neuropsychiatric disorders (Trubetskoy et al., 2022), play pivotal roles in spine formation, elimination, and remodeling during both development and adulthood (Li et al., 2017; Ting et al., 2012). While molecules that promote the formation and organization of dendritic spines have been extensively studied, the regulators that facilitate the elimination of spines, prevent their overgrowth, or restructure their morphology remain less well characterized.

Protocadherin 17 (PCDH17) belongs to the non-clustered δ2-protocadherin family and is expressed across various brain regions, including the basal ganglia, hippocampus, and cortex (Hoshina et al., 2013; Kim et al., 2010). PCDH17 participates in the regulation of axon extension and presynaptic vesicle assembly (Hayashi et al., 2016; Hoshina et al., 2013); however, its function in postsynaptic assembly remains poorly understood. Genome-wide association studies (GWAS) have identified rs9537793, a single-nucleotide polymorphism (SNP) within the gene that encodes PCDH17, as associated with major mood disorders (Chang et al., 2018). Furthermore, risk alleles are associated with elevated PCDH17 mRNA levels in postmortem brains, and patients with bipolar disorder exhibit higher levels of PCDH17 expression in the brain compared to healthy controls (Chang et al., 2018). Hence, dissecting the roles and underlying molecular mechanisms of PCDH17 in dendritic spine morphology and behavioral responses is critical for understanding the pathological effects of PCDH17 on mood disorders.

In the present study, we demonstrated that PCDH17, enriched in dendrites and postsynaptic sites of excitatory neurons, restricted the number and head size of mushroom spines in excitatory synapses in both cultured neurons and pyramidal neurons of hippocampal CA1 brain slices in mice. Conversely, PCDH17 knockdown increased the density and size of mushroom spines in cultured mouse neurons, effects that were abrogated by co-expressing human PCDH17. Viral-mediated overexpression of PCDH17 in hippocampal CA1 neurons led to anxiogenic and depression-like behaviors in mice. Characterization of the PCDH17-associated proteome revealed enrichment in proteins involved in actin cytoskeleton binding and regulation. Specifically, PCDH17 interacted with ROCK2, a Rho-associated protein kinase, and regulated levels of ROCK2-downstream targets such as LIMK1 and phospho-cofilin (pCofilin) serine-3 (Ser3), thereby modulating actin cytoskeleton organization. Furthermore, the effects of PCDH17 on spine density and morphology, as well as actin filament (F-actin) content, were restored by KD025 (belumosudil), a selective ROCK2 inhibitor (Lee et al., 2014). These findings suggest that PCDH17 contributes to the elimination of dendritic spines and modulates spine morphology through ROCK2-regulated actin cytoskeleton organization, elucidating a potential molecular mechanism by which PCDH17 influences spine pathology and regulates anxiety and depressive behaviors associated with mood disorders.

MATERIALS AND METHODS

Animals
Adult male C57BL/6J mice (8–12 weeks) were purchased from Hunan SJA Laboratory Animal Co., Ltd. (Changsha, China). All animals were housed under a 12 h light/dark cycle in a temperature (22–24°C) and humidity (40%–60%) controlled room with adequate food and water. This study was approved by the Ethics Review Committee for Animal Experimentation of Central South University (approval No. 2022-2-41). All efforts were made to minimize the number of subjects used and their suffering.

Plasmids
The plasmid pLifeAct_mScarlet_N1 was a kind gift from Dorus Gadella (Addgene plasmid, # 85054). The cDNA of PCDH17 was obtained by reverse transcription polymerase chain reaction (RT-PCR) and inserted into the Asc1 and Sal1 sites of the GW1-Myc (promoter: CMV) vector (Liao et al., 2022) using Gibson assembly, and into the EcoRI and XhoI sites of the pLenti-CAG-IRES-GFP vector (Addgene, #69047). To generate lentiviral vectors expressing PCDH17, the CaMK2α promoter and PCDH17 cDNA sequence were amplified from pAAV-CaMK2α-hChR2(H134R)-EYFP (Addgene, #26969) and the GW1-myc-PCDH17 construct, respectively, then cloned into the PacI/AgeI and BamHI/NheI sites of the pUltra-hot plasmid (Addgene, #24130). The primer sequences used included: PCDH17-AscI: ATATCTGAAGAGGACTTGGGATG TACCTTTCCATCTGTTG; PCDH17-Sal1: TGAATTCGATAT CCTGCAGGTCACTTTCTCACAGCCAC; CaMK2α-PacI: CCTTAATTAAGGTACATCAAGTGTATCATA; CaMK2α-AgeI: CCCACCGGTGGGGCTGCCCCCAGAACTAGG; PCDH17-BamHI: GAATCCCGGGCCTTCTAGAGCCATGTACCTTTCC ATCTGTTG; and PCDH17-NheI: GAACGAATTCTGAT CACACGTCACTTTCTCACAGCCAC.

To generate short hairpin RNA (shRNA) constructs, annealed oligoes containing the shRNA sequence against PCDH17 were inserted into the pSuper (promoter: H1) vector (OligoEngine). The shRNA sequences targeting mouse PCDH17 included: PCDH17-shRNA1: 5'-GGCGACGTGTC TATTTACA-3'; PCDH17-shRNA2: 5'-CCACCGTACAGATC GATCAATGT-3'; and PCDH17-shRNA3: 5'-GGTCAGAGGTG ATGTATCT-3'.

RNA interference
Small interfering RNA (siRNA) oligos were synthesized by GenePharma (China). The siRNA sequences targeting mouse ROCK2 included: ROCK2-siRNA1: 5'-GGUUUAUGCAAU GAAGCUUTT-3' and 5'-AAGCUUCAUUGCAUAAACCTT-3'; ROCK2-siRNA2: 5'-GCACUAGAAGAACACCUUAUT-3' and 5'-UAAGGUGUUCUUCUAGUGCTT-3'. The transfections were performed in antibiotic-free media using DharmaFECT DUO Transfection reagent in accordance with the manufacturer's instructions. ROCK2 silencing was performed by transfecting the siRNA (50 nmol/L) into N2a cells for 48 h.

Total RNA extraction and real-time RT-PCR (RT-qPCR)
For primary cultured neurons and N2a cells, total RNA was

extracted using TRIzol reagent in accordance with the manufacturer's protocols. Approximately 1 µg of total RNA was utilized for reverse transcription, and standard real-time RT-PCR assays were performed using SYBR Green (Vazyme, China) in triplicate. The RT-PCR analysis was performed in 96-well plates with a 10 µL reaction volume under the following thermal cycling conditions: 95°C for 15 min, followed by 35 cycles at 95°C for 15 s, 60°C for 30 s, and 72°C for 30 s. The results were analyzed using the ΔΔCt method. Gene expression levels were normalized to GAPDH expression. The primer sequences used included: PCDH17: 5'-GATT TGAACGCCACTGATGCT-3' and 5'-GGTTGCCCTTAA CGCGGAT-3'; ROCK2: 5'-TTGGTTCGTCATAAGGCATCAC-3' and 5'-TGTTGGCAAAGGCCATAATATCT-3'; cofilin (CFL1): 5'-ATGACATGAAGGTTCGCAAGT-3' and 5'-GAC AAAAGTGGTGTAGGGGTC-3'; LIMK1: 5'-TGTAGCGTC TCCCTTTCACAC-3' and 5'-ATCGCCAATGAAGTTTCCACA-3'; and GAPDH: 5'-AGGTCGGTGTGAACGGATTTG-3' and 5'-TGTAGACCATGTAGTTGAGGTCA-3'.

Primary neuronal culture

Mouse cortical and hippocampal neurons were cultured as described previously (Gao et al., 2022). In brief, E16.5–E17.5 embryos from pregnant mice were dissected in ice-cold Hank's Balanced Salt Solution (HBSS) under a dissection microscope. The isolated cortical and hippocampal tissues were twice washed with ice-cold HBSS, incubated with trypsin in HBSS at 37°C for 20 min with gentle shaking every 5 min, and digested in 5 mL of 0.025% trypsin. The trypsin-digested tissues were twice washed with warm HBSS to remove trypsin, followed by gentle trituration in glass Pasteur pipettes 10–15 times in neuronal culture medium (neurobasal medium supplemented with B27, GlutaMAX, and penicillin/streptomycin). Cells were filtered through a 70 µm Nylon cell strainer and counted using a hemocytometer. After resuspension in culture medium, the neurons were seeded onto 6- or 12-well cell culture plates coated with poly-D-lysine at 4–$6×10^5$ cells/mL for RNA and protein extraction, and 1–$2×10^5$ cells/mL for immunostaining. The neurons were maintained in neuronal culture medium at 37°C and 5% CO_2, with 35% of the medium replaced with fresh medium 4 days after plating.

DNA transfection and lentiviral transduction

HEK293T and N2a cells (both from ATCC) were cultured in Dulbecco's Modified Eagle Medium (DMEM) supplemented with 10% fetal bovine serum (FBS) and transfected using PEI reagent (Polysciences, USA). For imaging analyses, cultured neurons were transfected at 14 days in vitro (DIV14) using Lipofectamine 2000 reagent (Invitrogen, USA) according to the manufacturer's suggestions. All neuronal images were obtained at DIV18-19. For immunoblotting, cultured neurons were transduced with lentiviral particles at DIV4 and harvested at DIV18.

Pharmacological treatment

Cultured neurons and N2a cells were treated with belumosudil (KD025, 10 µmol/L, Selleckchem, S7936, USA) for 36–48 h, followed by immunofluorescence examination. The lentivirus-injected mice were treated with vehicle (CMC-Na) or KD025 by orogastric gavage for 3 consecutive days at doses of 150 mg/kg, twice daily.

Preparation of mouse brain samples

For histological analysis, mice were transcardially perfused with ice-cold 1×phosphate-buffered saline (PBS), followed by 4% paraformaldehyde (PFA). Brains were post-fixed in 4% PFA for 1 day and cryoprotected in 30% sucrose, followed by freezing and sectioning with a vibratome (Leica VT1000S, Germany). Serial free-floating coronal sections (70 µm) were collected, and anatomically matching sections were used for staining and analysis.

For protein extraction, hippocampi were carefully dissected, flash frozen in liquid nitrogen, and stored at −80°C until further use.

Immunoblotting

Immunoblotting was performed as described previously (Gao et al., 2022; Wang et al., 2023). Mouse tissues and cultured neurons were collected and homogenized in lysis buffer (50 mmol/L Tris-HCl with pH 7.4, 120 mmol/L NaCl, 5 mmol/L EDTA, 1% Nonidet P-40, 0.1% sodium deoxycholate, and 50 U/mL aprotinin). Protein concentrations were measured using a BCA protein assay kit (Thermo Fisher Scientific, USA). Lysates were resolved by sodium dodecyl-sulfate polyacrylamide gel electrophoresis (SDS-PAGE) and transferred to polyvinylidene difluoride membranes (Millipore, USA). The membranes were then blocked with 5% milk/0.1% Tween-20 in Tris-buffered saline for 1 h and blotted with primary antibodies at 4°C overnight. Horseradish peroxidase-Renaissance Plus Reagent (Thermo Fisher Scientific, USA) was used to visualize the immunoreactive proteins. The following antibodies were used: actin (1:5 000, Proteintech, 66009-1, USA), β3 tubulin (1:5 000, Millipore, mab1637, USA), GAPDH (1:2 000, Proteintech, 60004-1-lg, USA), Myc (1:1 000, MBL, M047-3, China), PCDH17 (1:1 000, Abcam, ab128815, UK), ROCK2 (1:1 000, Proteintech, 21645-1-AP, USA), LIMK1 (1:1 000, Proteintech, 67974-1-lg, USA), cofilin (1:1 000, Proteintech, 66057-1-lg, USA), pCofilin (Ser3) (77G2) (1:1 000, CST, mAb3313, USA), PSD95 (1:1 000, CST, 3450s, USA), synaptophysin (1:1 000, Abcam, ab32594, UK), and Flag (1:1 000, CST, 14793, USA).

Co-immunoprecipitation (co-IP)

Mouse brains were lysed with RIPA buffer (50 mmol/L Tris with pH 8.0, 1% Triton X-100, 0.1% SDS, and 150 mmol/L NaCl containing a protease inhibitor cocktail). Lysates were then centrifuged at 12 000 ×g for 25 min at 4°C. Antibodies (1 µg) were added to the cell lysates and incubated at 4°C for 2 h on a roller mixer, followed by incubation with Protein A Sefinose Resin (Sangon Biotech, China) pre-equilibrated in lysis buffer for 2 h at 4°C. N2a cell lysates transfected with pLenti-PCDH17-3×Flag plasmid were incubated with anti-FLAG M2 affinity gel (Sigma, USA) for 4 h. Immunoprecipitates were washed four times in lysis buffer, boiled in SDS sample buffer, and subjected to immunoblotting.

Immunofluorescence staining

For brain slices, immunofluorescence staining was carried out on free-floating 70-µm-thick sections as described previously (Gao et al., 2022). Sections were blocked with PBS containing 5% bovine serum albumin (BSA) and 0.3% Triton X-100 for 2 h at room temperature, followed by overnight incubation with primary antibodies at 4C°. Sections were washed with 1×PBS three times, incubated with secondary antibodies at room temperature for 2 h (1:200, Alexa Fluor 488, Alexa Fluor 555, Alexa Fluor 647, Jackson ImmunoResearch, USA), washed with 1×PBS, counterstained with 4',6-diamidino-2-phenylindole (DAPI), and mounted in Fluoromount-G

(SouthernBiotech, USA).

Primary cultured neurons at DIV18–19 and N2a cells were fixed with 4% formaldehyde/4% sucrose for 15 min, then washed three times with 1×PBS. All cells were incubated with primary antibodies overnight at 4°C, washed three times in 1×PBS, and incubated with secondary antibody for 1 h at room temperature. Neurons were visualized by co-transfection with plasmid expressing Venus/DsRed. The following antibodies were used: PCDH17 (1:1 000, Abcam, ab128815, UK), ROCK2 (1:1 000, Proteintech, 21645-1-AP, USA), cofilin (1:1 000, Proteintech, 66057-1-Ig, USA), pCofilin (Ser3) (77G2) (1:1 000, CST, mAb3313, USA), RFP (1:1 000, Rockland, 600-401-379, USA), NR2A (1:500, Millipore, 07-632, USA), Homer1 (1:500, Synaptic Systems, 160 011, Germany), LIMK1 (1:500, Proteintech, 67974-1-Ig, USA), CaMKα (1:500, Proteintech, 13730-1-AP, USA), and Alexa Fluor 555 phalloidin (Thermo Fisher, A34055, 1:1 000, USA).

Confocal microscopy and image analysis

Images were acquired on a ZEISS LSM900 confocal microscope with a Plan-Apochromat 63× NA 1.4 oil differential interference contrast objective lens. Quantification of dendritic spines in hippocampal brain slices and cultured neurons was performed with ImageJ software (NIH, USA). For analysis of fluorescence intensity in cell cultures, Z-stack confocal images were acquired at a 0.5 μm interval covering a thickness of 10 μm. Fluorescence signal intensity of the transfected cells was analyzed using Imaris (Bitplane, Switzerland) or ImageJ software (NIH, USA).

Lentiviral packaging

For lentiviral packaging, HEK293T cells were co-transfected with pUltra-CaMKα-mCherry-p2a-PCDH17 and pUltra-CaMKα-mCherry, along with psPAX2 (Addgene, #12260) and pMD2G (Addgene, #8454) using PEI reagent (Polysciences, USA). The cells were then cultured with DMEM containing 10% FBS. Medium containing lentiviral particles was collected twice at 2 and 3 days post-transfection. The lentivirus was purified by ultracentrifugation (Beckman, Rotor SW28, USA) at 4°C and 25 000 r/min for 2 h, then stored at −80°C for further experiments.

Stereotaxic injection

Male C57BL/6J mice (8–10 weeks old) were anesthetized with isoflurane (1%–2% mixed with air) and sterilized with iodophors and alcohol. Viral particles carrying pUltra-CaMKα-mCherry or pUltra-CaMKα-mCherry-p2a-PCDH17 (3 μL) were injected bilaterally into the hippocampal CA1 regions using the following coordinates: 2.9 mm posterior to bregma, 3.2 mm lateral to midline, and 4.0 mm below the brain surface at a rate of 200 nL/min using a microinjection system (World Precision Instruments, USA). The needle was kept in place for 10 min before withdrawal. The virus-injected mice were subjected to behavioral testing 10–14 days later.

Behavioral tests

All behavioral experiments were conducted blind using male C57BL/6J mice (8–12 weeks old).

Open field test (OFT): General motor activity was assessed using an OFT in a square arena (40 cm×40 cm×35 cm (width×depth×height)) constructed of polyvinyl chloride. Mice were positioned at the center of the test arena, and their activity was continuously recorded for 10 min using Activity Monitor software (Labmaze Animal Behavior Analysis Software v.3.0, China). Parameters such as distance (cm), speed (cm/s), and zone entries were automatically recorded and scored.

Y-maze test: Male mice were individually habituated to a Y-shaped maze (4 cm×10 cm×12 cm), featuring three opaque white plastic arms at 120° angles from each other. During the test, each mouse was allowed to freely explore the three arms for 6 min. It is expected that the mice would show a preference for entering less recently visited arms over the course of multiple arm entries. Number of arm entries and number of triads were recorded to calculate the percentage of alternation, with an entry counted when all four limbs of the mouse were within the arm.

Novel object recognition (NOR) task: The mice were individually habituated to an open field box (40 cm×40 cm×35 cm) for 1 day. During training, two novel objects were placed in the box and each mouse was allowed to explore for 6 min. The time spent exploring each object was recorded. During the retention tests, the mice were reintroduced to the same box, in which one of the familiar objects used during training was replaced by a novel object, and allowed to explore freely for 6 min. A preference index, calculated as the ratio of the amount of time spent exploring one of the two objects (training session) or novel object (retention session) over the total time spent exploring both objects, was used to measure recognition memory.

Light-dark transition test (LDT): The light-dark box consisted of two compartments: a transparent polyvinyl chloride box and a black polyvinylchloride box (both 19 cm×19 cm×19 cm). The two boxes were separated by a vertical sliding door that remained open (5 cm×5 cm). The activity of each mouse in the two compartments was monitored for 6 min. The amount of time spent in the transparent and black boxes was automatically measured.

Tail suspension test (TST): Mice were suspended above the floor by fixing the ends of their tails to wire netting. Immobility was observed and quantified over a 6 min test session.

Forced swim test (FST): Mice were placed in a cylinder filled with water at 23–25°C. Immobility was observed and quantified over a 6 min test session.

Marble burying test (MBT): A cage measuring 10 cm×20 cm was filled with 5 cm of corn kernel bedding, with 20 marbles neatly arranged in 4×5 rows on top. The test mice were placed into the cages and remained there for 30 min. The number of marbles each mouse buried into the bedding was counted.

Sucrose preference test (SPT): The mice were separately placed in test cages after 4–5 h of water deprivation. Each cage was then equipped with a bottle of ordinary drinking water and a bottle of 1% sucrose water. After 24 h, the volumes of ordinary water and sucrose water were counted.

Affinity purification using Myc pull-down on mouse brain tissue

pGW1-myc-PCDH17 and pGW1-myc were transfected into HEK293T cells using GenJet (SignaGen, USA). Myc pull-down was performed as described previously (Stucchi et al., 2018). After 48 h, the cells were lysed using pre-cooled RIPA buffer (50 mmol/L Tris with pH 8.0, 1% Triton X-100, 0.1% SDS, and 150 mmol/L NaCl containing a protease inhibitor cocktail). Protein A Sefinose Resin (Sangon Biotech, China) was incubated with Myc antibody (Cell Signaling Technology, USA) and 5% BSA at 4°C for 1.5 h to form a bead-antibody complex. The complex was then incubated with the cell lysate at 4°C for 1 h, followed by centrifugation at 6 500 r/min and

4°C for 5 min. The beads were washed twice in low-salt washing buffer (20 mmol/L Tris-HCl pH 7.4–7.8, 100 mmol/L KCl, 0.1% Triton X-100) and once in high-salt washing buffer (20 mmol/L Tris-HCl pH 7.4–7.8, 500 mmol/L KCl, 0.1% Triton X-100), followed by two final washes in low-salt washing buffer (20 mmol/L Tris-HCl pH 7.4–7.8, 0.1% Triton X-100). Additionally, brain tissues from 2-month-old C57BL/6J mice were washed in ice-cold PBS, lysed with RIPA buffer, incubated at 4°C for 30 min with rotation, and 13 000 r/min centrifuged at 4°C for 30 min. The resulting supernatants were incubated with beads previously conjugated with Myc-tagged proteins at 4°C for 2 h. The beads were then washed with RIPA buffer three times at 4°C, resuspended in 100 µL of SDT lysis buffer (4% SDS, 100 mmol/L Tris-HCl with pH7.5, 1 mmol/L DTT), and boiled at 95°C for 10 min.

Mass spectrometry and data analysis

Protein samples were quantified and digested using trypsin. Digested peptides from each sample were desalted using C18 cartridges (Empore™ SPE Cartridges C18, bed I.D. 7 mm, volume 3 mL, Sigma, USA), concentrated by vacuum centrifugation, and resuspended in 40 µL of 0.1% formic acid (v/v). Liquid chromatography-tandem mass spectrometry (LC-MS/MS) was performed on a Q Exactive mass spectrometer (Thermo Scientific, USA) coupled to an Easy-nLC system (Thermo Fisher Scientific, USA) for 60/120/240 min. Raw MS data for each sample were combined and searched against the Swiss-Prot and TrEMBL databases using MaxQuant v.1.5.3.17 for identification and quantitation analysis. The label-free quantification (LFQ) intensity method was used for protein quantification. Proteins exhibiting >2.5-fold-change in expression when comparing myc-PCDH17 versus control samples were identified as PCDH17-binding protein candidates and subjected to gProfiler Gene Ontology (GO) enrichment analysis and clustering analysis of enriched GO terms using Cytoscape EnrichmentMap (Reimand et al., 2019).

Statistical analysis

For each experiment, the corresponding statistical tests are indicated in the figure legends. The number of samples for each group is shown in the figure and figure legends. Statistical analysis was performed using GraphPad Prism v.9.0 (GraphPad Software, USA). Student's t-test was used to determine significant differences between two groups. One-way and two-way analysis of variance (ANOVA) with Dunn's or Fisher's least significant difference (LSD) *post hoc* tests were used to compare differences between three or more groups. All error bars indicate standard error of the mean (SEM). Significance levels were denoted at *: $P<0.05$, **: $P<0.01$, ***: $P<0.001$, and ****: $P<0.0001$.

RESULTS

PCDH17 functions at the postsynapse to inhibit dendritic spine density and size during development *in vitro*

Prior research has shown that PCDH17 is localized at synapses within the basal ganglia (Hoshina et al., 2013). Similarly, our biochemical fractionation of mice hippocampal tissue revealed that PCDH17, like synaptic proteins such as PSD95 and synaptophysin, was highly enriched in the P2 fraction, which resembles the crude synaptosome (Figure 1A). Immunofluorescence of cultured excitatory neurons at DIV18 indicated that PCDH17 puncta were distributed along the

dendritic shaft and co-localized with Homer1, a postsynaptic scaffold protein in excitatory neurons (Figure 1B, C, Pearson's correlation coefficient of PCDH17/Homer1=0.243). These findings suggest that PCDH17 is present at the dendritic shafts and postsynaptic sites of forebrain excitatory neurons.

To investigate the effects of PCDH17 on the density and morphology of dendritic spines, cultured mouse cortical neurons (DIV14) were co-transfected with the GW1-myc-PCDH17 construct or control vector, along with a construct expressing Venus (a YFP variant) for visualization of neuronal morphology. At 4 days post-transfection, dendritic spine densities were quantified. Results indicated that PCDH17 overexpression led to a decrease in the overall density of dendritic spines, including a significant reduction in the density of mushroom-like spines, which represent the mature form of dendritic spines (Figure 1D, E, 6.447±0.2968 total spines/10 µm in control neurons, 5.327±0.2477 total spines/10 µm in PCDH17-overexpressing neurons, $P=0.0069$; 2.225±0.1776 mushroom spines/10 µm in control neurons, 1.212±0.1077 mushroom spines/10 µm in PCDH17-overexpressing neurons, $P=3.25×10^{-5}$). The densities of stubby spines, thin spines, and filopodium decreased slightly or remained unchanged in PCDH17-overexpressing neurons compared to control neurons, (Figure 1E, stubby: 2.022±0.1323 spines/10 µm in control neurons, 1.997±0.1601 spines/10 µm in Myc-PCDH17 neurons, $P=0.9063$; thin: 0.9011±0.0787 spines/10 µm in control neurons, 0.912±0.1056 spines/10 µm in Myc-PCDH17 neurons, $P=0.9336$; filopodium: 1.349±0.0929 spines/10 µm in control neurons, 1.206±0.0779 spines/10 µm in Myc-PCDH17 neurons, $P=0.2497$; $n=18$–20). Elevated PCDH17 expression also resulted in a reduction in both the size and head width of mushroom spines (Figure 1F, mushroom area: 0.8005±0.0572 µm^2 in control neurons; 0.6215±0.0343 µm^2 in Myc-PCDH17 neurons, $n=12$, $P=0.0136$; mushroom head: 1.065±0.0339 µm in control neurons; 0.9448±0.0352 µm^2 in Myc-PCDH17 neurons, $n=12$, $P=0.0224$), suggesting that excessive PCDH17 levels contribute to spine shrinkage. Similar effects on the loss of dendritic spine types were observed in cultured hippocampal neurons (Supplementary Figure S1A, B), with the density and size of mushroom spines showing the most substantial reductions following PCDH17 overexpression (Supplementary Figure S1B–D).

Given that primary cultured excitatory neurons from the hippocampus and cortex exhibit similar morphology and molecular signaling (Gao et al., 2022; Hu et al., 2014), and that PCDH17 affects dendritic spine number in both regions, we utilized mixed cultured neurons dissociated from these two regions for subsequent study. Immunostaining with antibodies against Homer1 and NR2A, two postsynaptic proteins, revealed that neurons transfected with the PCDH17 construct contained fewer Homer1 and NR2A puncta on dendrites compared to those transfected with control vectors (Figure 1G, H–J). In contrast, the signal intensity of PCDH17 showed an approximate 2.2-fold increase in neurons transfected with the PCDH17 construct compared to those transfected with the empty control vector (Figure 1H). These findings suggest that PCDH17 restricts the localization of postsynaptic proteins at the dendrites.

We next tested whether PCDH17 expression is involved in postnatal neuronal development. Notably, PCDH17 protein expression in the mouse hippocampus increased from postnatal days 1 to 21 and then slightly decreased thereafter (Figure 1K, L), coinciding with the postnatal developmental
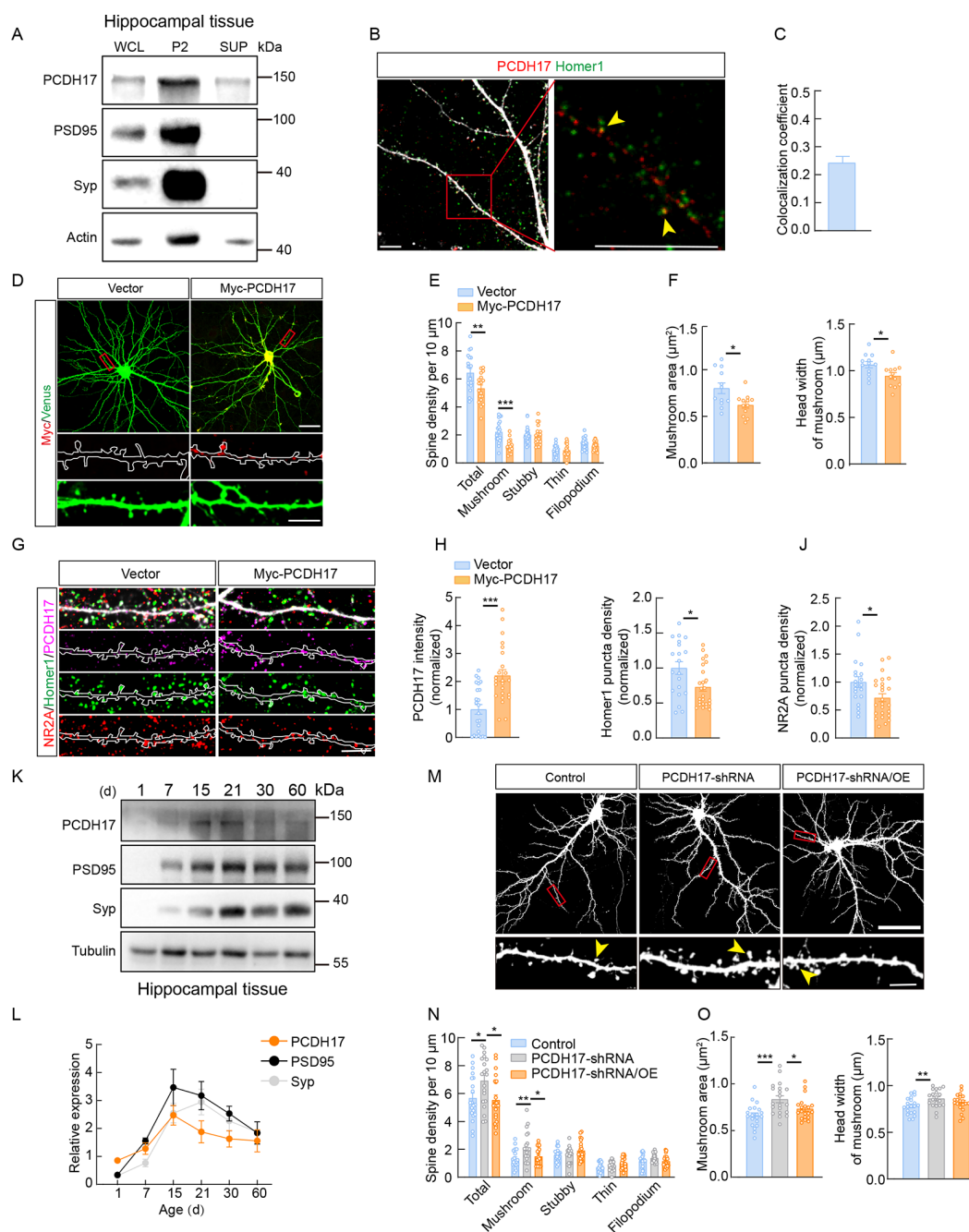
Figure 1 PCDH17 regulates spine density and morphology in primary dissociated neurons

A: Western blot analysis of PCDH17, PSD95, and Syp in WCL (whole-cell lysis), P2 (crude synaptosome), and SUP (supernatant). Syp: Synaptophysin. B: Representative images of immunostaining for PCDH17 (Red) and Homer1 (Green) in cultured neurons. Red boxes indicate dendrites in high-magnification images. Scale bars: Left, 5 μm; Right, 10 μm. Yellow arrowhead indicates colocalization of PCDH17 and Homer1. C: Pearson's correlation coefficients of PCDH17 and Homer1 in images from B were analyzed using ImageJ software. D: Representative confocal images of cultured neurons. Neurons were transfected with designated constructs along with Venus at DIV14, then imaged at DIV18. Red boxes indicate dendrites in high-magnification images. White lines show immunostaining of Myc-PCDH17 alongside Venus signal. Scale bars: Top, 20 μm; Bottom, 5 μm. E: Quantitative analysis of spine density at secondary dendrites in cultured neurons from D. n=18–20 neurons per group. Student's t-test. F: Quantitative analysis of size and head width of mushroom spines at secondary dendrites in cultured neurons from D. n=12 neurons per group. Student's t-test. G: Representative images of immunostaining for PCDH17 (Magenta), NR2A (Red), and Homer1 (Green) in cultured neurons. White lines show analyzed dendrites. H–J: Quantitative analysis of signal intensity for PCDH17, Homer1, and NR2A from experiments in G. n=20–25 neurons per group. Student's t-test. K, L: Western blot analysis (K) and quantification (L) of PCDH17, PSD95, and Syp at indicated ages. Syp: synaptophysin. n=3–6 per group. M: Representative confocal images of cultured neurons. Neurons were transfected with designated constructs along with Venus at DIV14, then imaged at DIV18. Red boxes indicate dendrites in high-magnification images. OE: Overexpression of human PCDH17. Yellow arrowhead indicates mushroom spines. Scale bars: Top, 20 μm; Bottom, 5 μm. N: Quantitative analysis of spine density of secondary dendrites in cultured neurons from M. n=20–22 neurons per group. One-way ANOVA and Dunn's test. O: Quantitative analysis of size and head width of mushroom spines of secondary dendrites in cultured neurons from M. n=20 neurons per group. One-way ANOVA and Dunn's test. Data are mean±SEM. *: P<0.05; **: P<0.01; ***: P<0.001.

timeline of the hippocampus. To mitigate the developmental increase in PCDH17 levels, we generated constructs expressing shRNA against mouse PCDH17 and assessed their knockdown efficiency (Supplementary Figure S2A). Cultured neurons were transfected with the construct expressing the most effective shRNA (#3) or a control vector, along with a Venus construct at DIV14. Quantitative analysis of dendritic spines from neurons at DIV18 indicated that PCDH17 knockdown resulted in an increase in total spine density, as well as the density, area, and head width of mushroom spines (Figure 1M, O; Supplementary Figure S2B-E, 5.679±0.3638 total spines/10 μm in control neurons, 6.922±0.3958 total spines/10 μm in PCDH17 shRNA-transfected neurons, P=0.0263; 1.311±0.1418 mushroom spines/10 μm in control neurons, 2.141±0.2435 mushroom spines/10 μm in PCDH17 shRNA-transfected neurons, P=0.0055; n=20–21). Notably, these increases were negated by co-transfection with a construct expressing human PCDH17 (Figure 1M–O), which is resistant to PCDH17 shRNA (Supplementary Figure S2F, G), thus confirming that the effects of PCDH17 shRNA were due to PCDH17 knockdown.

Having demonstrated that PCDH17 regulates synapse development, we performed Sholl analysis to assess its effect on dendritic development. Results showed that the number of dendritic intersections was reduced in neurons transfected with PCDH17 compared to those transfected with control plasmid (Supplementary Figure S3), suggesting that PCDH17 overexpression decreases dendritic complexity during neuronal development.

Taken together, these findings indicate that PCDH17 acts as an inhibitor of spine development and morphogenesis, with its up-regulation during postnatal neuronal development restraining dendritic spine overgrowth and maintaining the appropriate number of synaptic connections.

Viral-mediated expression of PCDH17 leads to spine loss and shrinkage in the hippocampal circuit

To determine the postsynaptic role of PCDH17 on spine number and morphology within intact neuronal circuits, we generated a lentiviral construct expressing PCDH17 and mCherry (a red fluorescent protein) under the control of the CaMK2α promoter specific for forebrain excitatory neurons (Figure 2A, B). Lentiviral particles expressing PCHD17 and mCherry (Lv-PCDH17) and control viral particles expressing only mCherry (Lv-Ctrl) were stereotactically injected into the ventral hippocampal (vHPC) CA1 area of 2-month-old C57BL/6J mice (Figure 2C, D). At 30 days post-injection, hippocampal brain slices were prepared, and dendritic spines were analyzed. The specificity of lentivirus-mediated gene expression in excitatory neurons was validated via immunostaining with a CaMK2α antibody (Figure 2E). Analysis revealed that hippocampal neurons transduced with Lv-PCDH17 contained fewer dendritic spines on their apical dendrites compared to those transduced with Lv-Ctrl (Figure 2F, G, 4.207±0.2855 total spines/10 μm in Lv-Ctrl neurons, 2.454±0.2119 spines/10 μm in Lv-PCDH17 neurons, P=0.0011; n=5 mice). Moreover, the density of mushroom and stubby spines on apical dendrites was significantly reduced in Lv-PCDH17-infected neurons compared to Lv-Ctrl-infected neurons (Figure 2F, G, 2.166±0.1115 mushroom spines/10 μm in Lv-Ctrl neurons, 1.128±0.0198 mushroom spines/10 μm in Lv-PCDH17 neurons, P=1.62×10^{-5}; 1.269±0.0867 stubby spines/10 μm in Lv-Ctrl neurons, 0.7116±0.1645

stubby spines/10 μm in Lv-PCDH17 neurons, P=0.0172; n=5 mice).

Overexpression of PCDH17 in the vHPC results in anxiogenic and depressive behavior in mice

An earlier study reported that PCDH17 is genetically associated with major mood disorders, with higher expression correlated with risk alleles and detected in postmortem brains of patients with mood disorders (Chang et al., 2018). Here, we further investigated whether PCDH17 influences mood-related behavioral responses in mice. To increase PCDH17 expression in pyramidal neurons within the vHPC CA1, a critical area for emotion regulation, we performed bilateral intrahippocampal injections of Lv-PCDH17 into the vHPC CA1 of 2-month-old wild-type C57BL/6J mice. At 10 days post-injection, we assessed emotion-related activities of these mice based on various behavioral tests. In the OFT, mice injected with Lv-PCDH17 traveled shorter distances, spent less time in the center area of the test arena, and entered the central area less frequently compared to mice injected with Lv-Ctrl (Figure 3A–D). However, the total distance traveled and average speeds in the arena were comparable between the two groups (Figure 3E). These findings suggest that overexpression of PCDH17 in vHPC CA1 pyramidal neurons enhances anxiety levels and innate fear in mice, without affecting locomotor activity. In line with these results, in the MBT, widely used to assess anxiety-like behavior (Kedia & Chattarji, 2014; Njung'e & Handley, 1991), mice injected with Lv-PCDH17 buried substantially more marbles than those injected with Lv-Ctrl (Figure 3F, G), further supporting the anxiogenic effect of PCDH17 overexpression. In the LDT, Lv-PCDH17-infected mice spent less time in the light box than Lv-Ctrl-infected control mice, although this difference did not reach statistical significance (Figure 3H, P=0.1186).

The mice were next subjected to SPT, TST, and FST to evaluate the effect of PCDH17 overexpression on depression-like behaviors. SPT is commonly used to assess anhedonic behavior in patients with depression (Liu et al., 2018). Here, mice injected with Lv-PCDH17 consumed slightly less sucrose (Figure 3I, P=0.1512), suggesting that PCDH17 overexpression in the vHPC CA1 only has a subtle effect on anhedonia. Notably, in the TST and FST, mice injected with Lv-PCDH17 exhibited a marked increase in total immobility time and a reduction in the latency to first immobility compared to those injected with Lv-Ctrl (Figure 3J, K). These findings suggest that elevated expression of PCDH17 in the vHPC is associated with depressive behavior, particularly increased despair in response to an acute inescapable stress.

In addition, memory performance in PCDH17-overexpressing mice was examined using the spontaneous Y-maze test to assess spatial working memory and the NOR task to measure recognition memory. In the Y-maze test, alternation scores were similar between the Lv-PCDH17- and Lv-Ctrl-infected mice (Supplementary Figure S4A), suggesting intact spatial working memory after PCDH17 overexpression in the vHPC. In the NOR task, mice injected with either Lv-PCDH17 or LV-Ctrl spent comparable amounts of time in the zone containing novel objects and exhibited similar discrimination indices (Supplementary Figure S4B). Thus, increased expression of the PCDH17 protein in the vHPC does not appear to impact spatial working memory or object recognition memory.
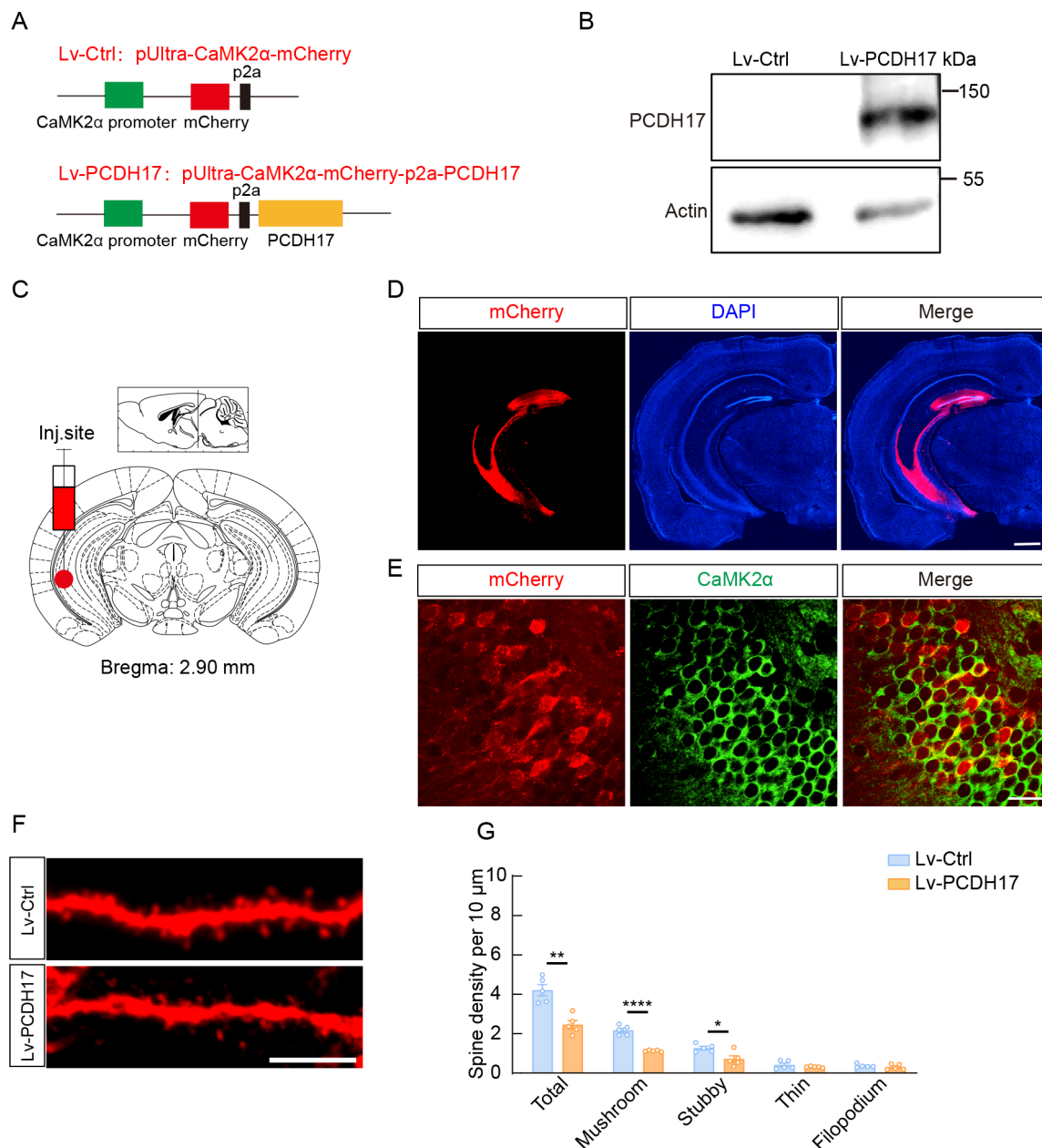
Figure 2 PCDH17 overexpression reduces spine density in hippocampus *in vivo*

A: Diagram of lentivirus construct expressing PCDH17 and mCherry (Lv-PCDH17) or mCherry alone (Lv-Ctrl) under control of CaMK2α promoter. B: Western blot analysis of PCDH17 expression. HEK293T cells were transfected with Lv-Ctrl or Lv-PCDH17 plasmids and maintained for 2 days before western blotting. C: Diagram of ventral hippocampus (vHPC) region in which lentiviral particles were injected, anatomical references adapted from Paxinos and Franklin's Mouse Brain in Stereotaxic Coordinates. D: Representative images of vHPC after lentiviral injection. Scale bar: 500 μm. E: Representative images of immunostaining for CaMK2α (Green) in the vHPC CA1 of mice injected with designated viral particles. Scale bar: 20 μm. F: Confocal images of secondary dendrites in the vHPC CA1 of mice injected with designated viral particles. Scale bar: 5μm. G: Quantitative analysis of spine density of secondary dendrites in neurons from F. n=5 mice per group. Data are mean±SEM. *: P<0.05; **: P<0.01; ****: P<0.0001, Student's *t*-test.

Characterization of PCDH17 interactome reveals that PCDH17 largely binds to actin cytoskeleton-related proteins

To explore the molecular interactors through which PCDH17 modifies spine number and morphology, we conducted a systematic affinity purification-mass spectrometry (AP-MS) screening (Stucchi et al., 2018) with PCDH17. Myc-PCDH17 was expressed in HEK293T cells, purified with Myc antibody-conjugated Protein A Sefinose Resin, and incubated with mouse brain lysates (Supplementary Figure S5A, B). The co-immunoprecipitated proteins were subjected to MS analysis,

resulting in the identification of 730 putative PCDH17-interacting proteins (Supplementary Table S1). To further understand the PCDH17 interactome, we performed gProfiler GO enrichment analysis and subsequent clustering analysis of enriched GO terms using Cytoscape EnrichmentMap (Reimand et al., 2019). Notably, highly enriched clusters in the PCDH17 interactome included proteins related to "postsynaptic structure maintenance behavior" and "vesicle transmembrane secretion monoatomic", consistent with its postsynaptic localization observed in our study and its presynaptic role reported in earlier studies (Hayashi et al.,
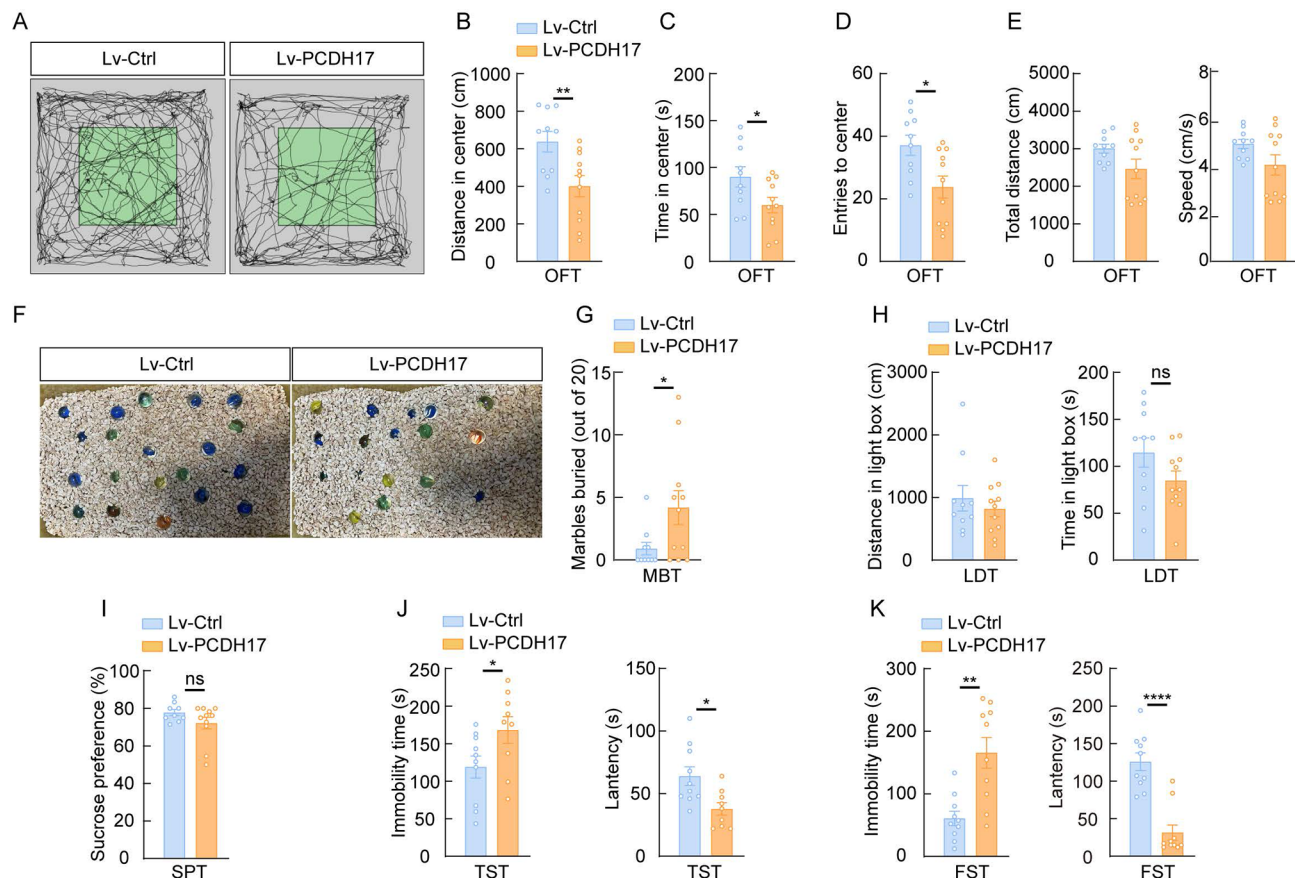
Figure 3 vHPC-specific overexpression of PCDH17 leads to abnormal mood behaviors in mice

A: Representative traits of mouse in open field test (OFT). B–E: Quantification of distance in center (B), time in center (C), entries in center (D), total travel distance, and average speed (E) in OFT. n=10–11 mice per group. F: Representative images of marble burying test (MBT). G: Quantification of number of marbles buried by each mouse. n=10–11 mice per group. H: Quantification of distance and time in light-dark transition (LDT). n=10–11 mice per group. I: Quantification of sucrose preference index in sucrose preference test (SPT). n=10–11 mice per group. J: Quantification of immobility time and latency to first observation of immobility in tail suspension test (TST). n=10–11 mice per group. K: Quantification of immobility time and latency to first observation of immobility in forced swim test (FST). n=10–11 mice per group. Data are mean±SEM. ns: No significance; [*]: P<0.05; [**]: P<0.01; [****]: P<0.0001, Student's t-test.

2016; Hoshina et al., 2013). Additionally, enriched clusters also included "actin microtubule organization cytoskeleton" (Figure 4A, B). Actin cytoskeletons are crucial for supporting dendritic spine structure and regulating spine formation and morphology, which are involved in mood and memory performance and neuropsychiatric disorders (Dillon & Goda, 2005; Ting et al., 2012; Yan et al., 2016). Furthermore, the clustered network contained highly enriched terms related to the actin cytoskeleton, such as "actin filament-base process", "actin cytoskeleton organization", and "regulation of actin polymerization or depolymerization", suggesting that PCDH17 interacts with proteins that regulate actin filament (F-actin) polymerization or depolymerization to modify F-actin dynamics, thereby affecting spine number and morphology.

To explore this hypothesis, we transfected cultured neurons (DIV14) with a PCDH17 construct and subsequently stained F-actin using phalloidin. Results showed that PCDH17-transfected neurons displayed decreased levels of dendritic F-actin and smaller F-actin puncta compared to control plasmid-transfected neurons (Figure 4C–E). Additionally, we co-transfected cultured neurons with PCDH17 or control plasmids, along with a construct expressing LifeAct-mScarlet, which specifically binds to and labels F-actin (Riedl et al., 2008). At 4 days post-transfection, quantitative analysis of LifeAct-mScarlet fluorescence signals revealed that signal intensity and the density and size of LifeAct-mScarlet puncta at the spines or along the dendritic shaft were markedly decreased in neurons transfected with the PCDH17 construct compared to those transfected with the control vector (Figure 4F–I). Collectively, these results demonstrate that PCDH17 overexpression leads to a reduction in F-actin content in neurons, confirming its role in actin cytoskeleton organization.

PCDH17 physically interacts with ROCK2

Among the putative PCDH17-interacting proteins, Rho-associated protein kinase 2 (ROCK2) and its known downstream targets, such as LIMK1 and cofilin, are recognized as essential regulators of actin dynamics (Dillon & Goda, 2005; Lin & Koleske, 2010; Maekawa et al., 1999; Tada & Sheng, 2006). Furthermore, overexpression of ROCK2 has been shown to enhance LIMK1 phosphorylation, leading to spine loss in neurons (Henderson et al., 2019). Here, we sought to investigate whether PCDH17 colocalizes and interacts with ROCK2. Co-immunostaining of cultured neurons at DIV18 with PCDH17 and ROCK2 antibodies indicated endogenous co-localization at the dendrites and spines (Figure 5A, B, Pearson's correlation coefficient of PCDH17 and ROCK2=0.243).

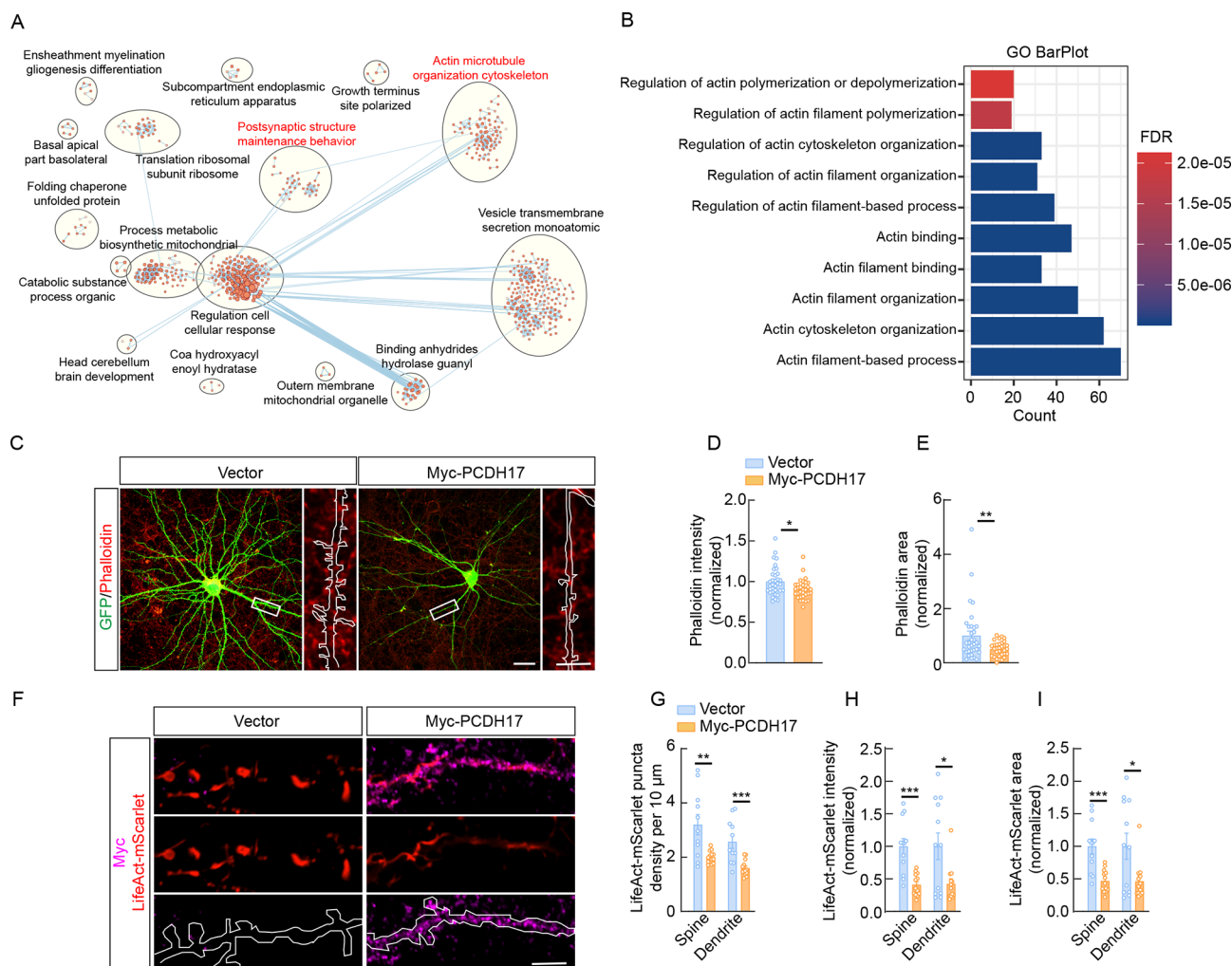We next assessed the interaction between PCDH17 and

Figure 4 PCDH17 is associated with proteins related to actin cytoskeleton and modules actin filaments

A: Map of gProfiler GO enrichment analysis of 730 putative PCDH17-interacting proteins. Node cutoff, *P*<0.01 and FDR<0.05; edge cutoff, overlap coefficient >0.5, Note, enriched clusters of "actin microtubule organization cytoskeleton" and "postsynaptic structure maintenance behavior" are labeled in red. B: Top 10 enriched GO terms associated with actin cytoskeleton based on gProfiler GO enrichment analysis. C: Representative images for phalloidin (Red) staining in cultured neurons. Neurons were transfected with designated constructs along with Venus at DIV14, then imaged at DIV18. White boxes indicate dendrites in high-magnification images. White lines show immunostaining of Myc-PCDH17 alongside Venus signal. Scale bars: Left, 10 μm; Right, 5 μm. D, E: Phalloidin intensity (D) and puncta area (E) of secondary dendrites in cultured neurons were analyzed using ImageJ software. *n*=32–34 neurons per group. F: Representative images for LifeAct-mScarlet (Red) in cultured neurons. Neurons were cotransfected with PCDH17 or control plasmids, along with a construct expressing LifeAct-mScarlet at DIV14. Neurons were fixed after 4 days and imaged using confocal microscopy. Scale bar: 10 μm. G: Quantitative analysis of density of LifeAct-mScarlet puncta at spines and dendrites in cultured neurons from F. *n*=11–13 neurons per group. H, I: Quantitative analysis of LifeAct-mScarlet signal intensity and area at spines and dendrites in cultured neurons from F. *n*=11–13 neurons per group. Data are mean±SEM. *: *P*<0.05; **: *P*<0.01; ***: *P*<0.001, Student's *t*-test.

ROCK2 *in vitro* using co-IP assays on N2a cells transfected with a PCDH17-3xFlag construct. Results demonstrated that PCDH17 robustly co-immunoprecipitated with ROCK2 in the N2a cells (Figure 5C). Moreover, endogenous PCDH17 and ROCK2 proteins were co-immunoprecipitated using a ROCK2 antibody from the hippocampal homogenates harvested from adult wild-type C57BL/6J mice (Figure 5D). These findings support the hypothesis that PCDH17 directly interacts with ROCK2.

PCDH17 modulates ROCK2 and its downstream molecules

To determine whether PCDH17 regulates the protein expression of ROCK2 and its downstream molecules, we transduced cultured neurons with lentivirus Lv-PCDH17, achieving a 3.6-fold increase in PCDH17 protein levels

(Figure 6A, B). Immunoblotting revealed that PCDH17 overexpression had a minor effect on ROCK2 levels in DIV14 neurons (Figure 6A, B). However, ROCK2 protein levels were significantly increased in DIV18 neurons transduced with Lv-PCDH17 compared to those transduced with Lv-Ctrl (Figure 6C, D). Similarly, immunostaining of cultured neurons (DIV18) and N2a cells indicated that cells transfected with the PCDH17 construct exhibited increased ROCK2-immunoreactive signal intensity compared to those transfected with the control vector (Figure 6E–H). Immunoblotting also confirmed that PCDH17 overexpression increased ROCK2 expression levels in N2a cells (Figure 6I, J). ROCK2 expression was also up-regulated in hippocampal slices from mice injected with Lv-PCDH17 compared to those injected with Lv-Ctrl (Figure 6K, L). Thus, increased expression of PCDH17 enhances ROCK2 protein levels both *in vitro* and
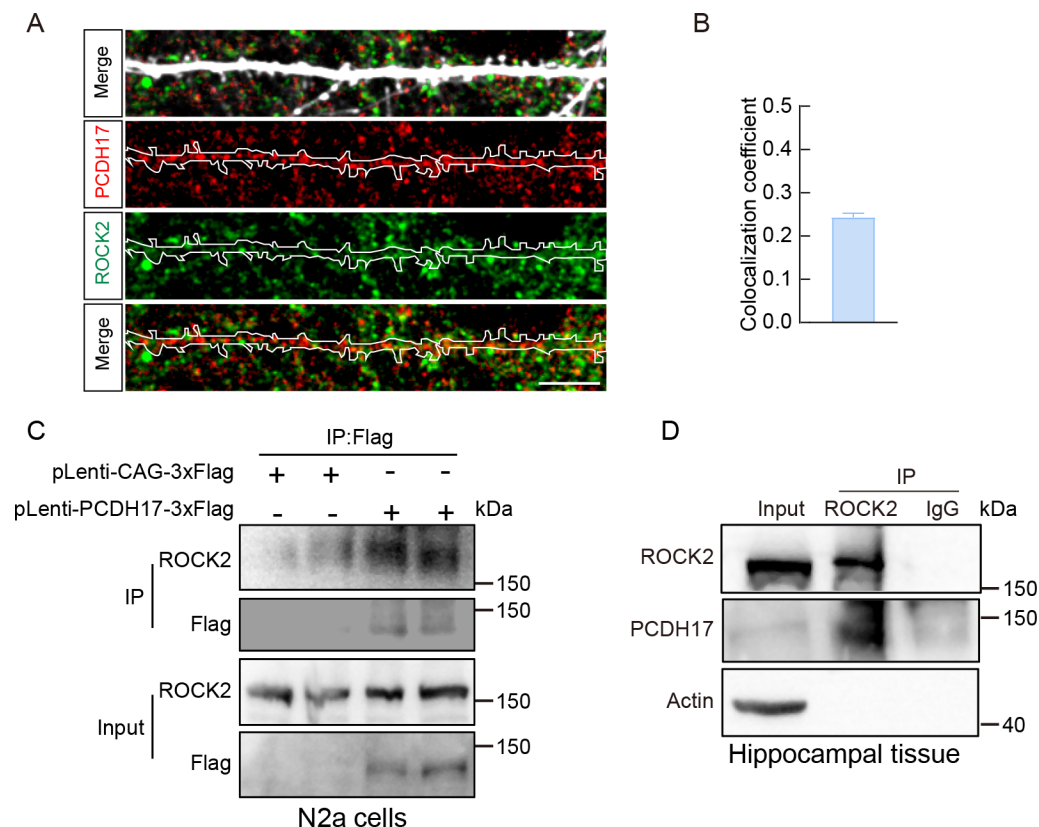
Figure 5 PCDH17 binds and colocalizes with ROCK2

A: Representative images of immunostaining in cultured neurons detecting endogenous PCDH17 (Red) and ROCK2 (Green). Scale bar: 10 µm. B: Pearson's correlation and overlap coefficient analysis of endogenous PCDH17 and ROCK2 from images in C. C: Co-immunoprecipitation of PCDH17 and endogenous ROCK2 in N2a cells transfected with Flag-tagged human PCDH17, with cells transfected with empty vector serving as a negative control. D: Co-immunoprecipitation of endogenous ROCK2 and PCDH17 in hippocampal tissue extracts from two-month-old wild-type mice, with normal IgG serving as a negative control.

in vivo.

We next examined the ROCK2 downstream molecular changes induced by PCDH17 overexpression. ROCK2 is known to regulate many signaling molecules associated with actin cytoskeleton and spine formation (Lin & Koleske, 2010; Peng et al., 2019; Zhou et al., 2009). As elevated ROCK2 expression reduces spine number via the serine and threonine kinase LIMK1 (Henderson et al., 2019), which controls the activity of cofilin, an actin depolymerization protein, by phosphorylating its Ser3 residue (Maekawa et al., 1999), we examined the effects of PCDH17 on LIMK1 and cofilin. Cultured neurons were transduced with Lv-PCDH17 and Lv-Ctrl viruses, followed by analysis of the protein levels of ROCK2 downstream molecules by immunoblotting (Figure 6M, O, Q). Levels of LIMK1 and pCofilin (Ser3), but not cofilin, were up-regulated in DIV18 neurons infected with Lv-PCDH17 compared to those infected with Lv-Ctrl (Figure 6M-R). Likewise, immunostaining indicated that the increase in PCDH17 expression in N2a cells transfected with the PCDH17 plasmid substantially enhanced LIMK1 and pCofilin (Ser3) levels, without altering cofilin levels (Figure 6S-V). The increase in pCofilin (Ser3) levels in PCDH17-overexpressing cells corroborates previous findings that heightened pCofilin (Ser3) impairs spine formation (Parisiadou et al., 2014).

To further explore the mechanism by which PCDH17 increases ROCK2 expression, we tested whether PCDH17 changes ROCK2 expression at the transcriptional level. We transduced Lv-PCDH17 and control viruses into cultured neurons (DIV5) and performed RT-qPCR at DIV18 to evaluate the effect of PCDH17 overexpression on mRNA levels of ROCK2 and its downstream molecules. Results indicated that transduction of the Lv-PCDH17 virus led to an up-regulation in the mRNA levels of PCDH17, but not of ROCK2, LIMK1, or CFL1 (cofilin) (Figure 6W). Thus, these findings suggest that PCDH17 regulates ROCK2 expression at the post-transcriptional level.

Pharmacological inhibition of ROCK2 alleviates defects in F-actin and spine formation caused by PCDH17 overexpression

Having established that PCDH17 binds to ROCK2 and regulates its downstream signaling, we further explored the role of ROCK2 in PCDH17-induced defects in F-actin and spine morphology. We transfected N2a cells with PCDH17 and control plasmid and treated the cells with KD025, a ROCK2-specific inhibitor (Lee et al., 2014). Consistent with the findings in cultured neurons, N2a cells transfected with PCDH17 exhibited remarkable reduction in phalloidin intensity and area, further supporting the notion that PCDH17 reduces F-actin content (Figure 7A–C). In cells transfected with the control vector, KD025 treatment enhanced F-actin accumulation (Figure 7A–C), suggesting that suppression of ROCK2 activity modulates actin cytoskeleton organization under normal physiological conditions. In cells transfected with the PCDH17 construct, in which ROCK2 signaling was activated, KD025 treatment markedly increased phalloidin
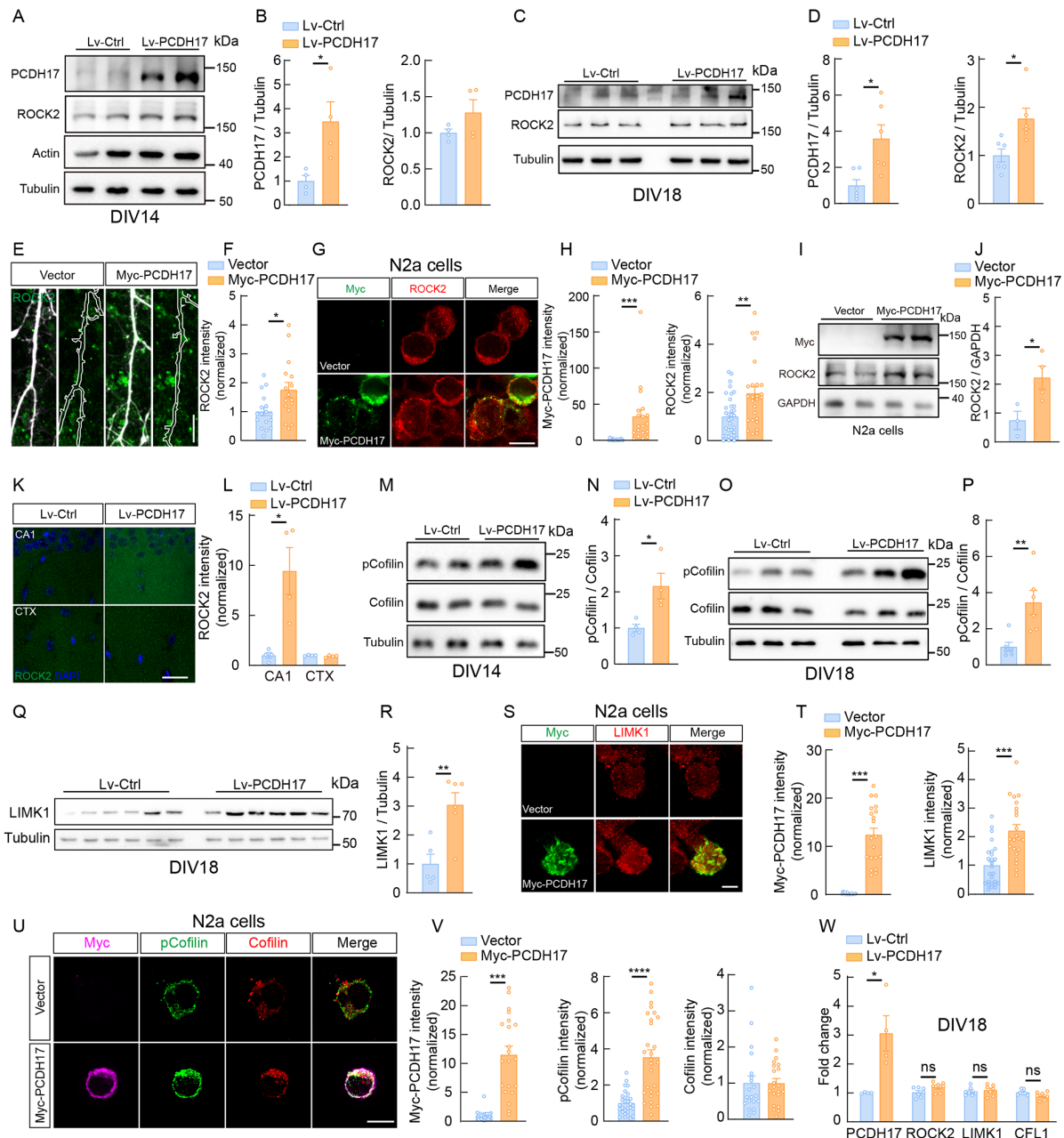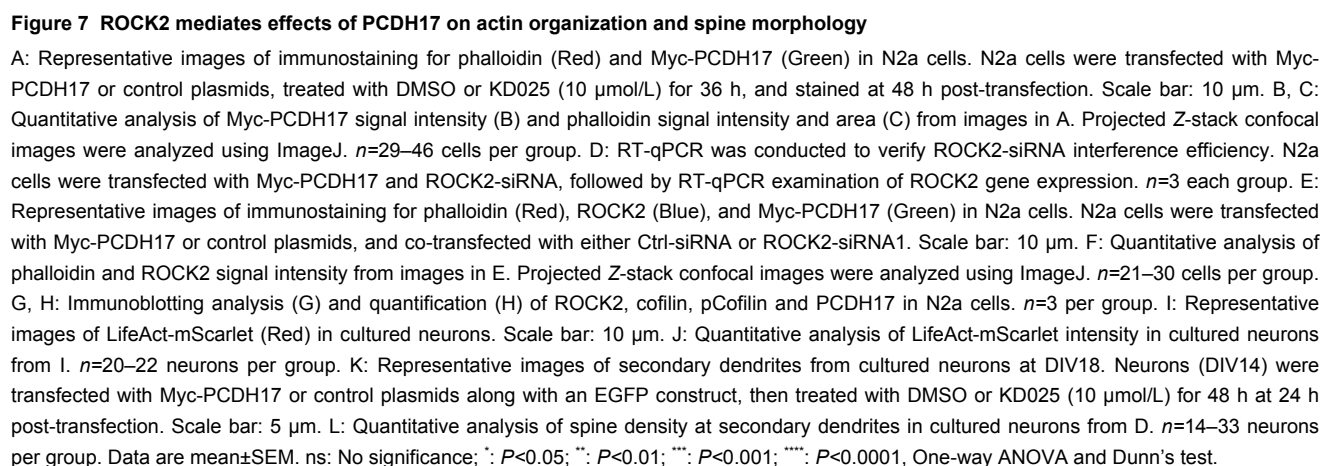
Figure 6 PCDH17 alters ROCK2 signaling pathway

A, B: Immunoblotting analysis (A) and quantification (B) of PCDH17 and ROCK2 in cultured neurons (DIV14). *n*=4 per group. C, D: Immunoblotting analysis (C) and quantification (D) of PCDH17 and ROCK2 in cultured neurons (DIV18). *n*=6 per group. E: Representative images of immunostaining for ROCK2 (Green) in cultured neurons. Neurons were transfected with Myc-PCDH17 or control plasmids. Scale bar: 10 μm. F: Quantitative analysis of ROCK2 signal intensity in cultured neurons using ImageJ. *n*=16–17 neurons per group. G: Representative images of immunostaining for ROCK2 (Red) and Myc-PCDH17 (Green) in N2a cells. Cells were transfected with Myc-PCDH17 or control plasmids. Scale bar: 10 μm. H: PCDH17 and ROCK2 signal intensities in N2a cells were analyzed using ImageJ. *n*=26–35 cells per group. I, J: Immunoblotting analysis (I) and quantification (J) of ROCK2 in N2a cells. *n*=3 per group. K, L: Confocal images (K) and quantitative analysis (L) of immunostaining for ROCK2 (Green) in hippocampal CA1 region of mice at 2 months of age. CTX: Cortex. Scale bar: 10 μm. Projected *Z*-stack confocal images were analyzed for intensity of ROCK2 using ImageJ, *n*=4 mice per genotype. M–P: Immunoblotting analysis (M, O) and quantification (N, P) of cofilin and pCofilin in cultured neurons on DIV14 (M, N) and DIV18 (O, P). *n*=4 per group. Q, R: Immunoblotting analysis (Q) and quantification (R) of LIMK1 in cultured neurons on DIV18. *n*=6 per group. S, T: Representative images of immunostaining of LIMK1 (Red) and Myc-PCDH17 (Green) in N2a cells (S). Cells were transfected with Myc-PCDH17 or control plasmids. Scale bar: 10 μm. PCDH17 and LIMK1 signal intensities in N2a cells were analyzed using ImageJ (T). *n*=22–26 cells per group. U, V: Representative images of immunostaining for cofilin (Red), pCofilin (Green), and Myc-PCDH17 (Magena) in N2a cells (U). Cells were transfected with PCDH17 or control plasmids. Scale bar: 10 μm. PCDH17, cofilin, and pCofilin signal intensities in N2a cells were analyzed using ImageJ (V). *n*=28–30 cells per group. W: Primary cultured neurons were infected with Lv-PCDH17 or control viruses, followed by RT-qPCR examination of PCDH17, ROCK2, LIMK1, and cofilin (CFL1) gene expression. *n*=4–7 treatments from three independent cultures for each group. Data are mean±SEM. ns: No significance; *: *P*<0.05; **: *P*<0.01; ***: *P*<0.001; ****: *P*<0.0001, Student's *t*-test.

www.zoores.ac.cn

Figure 7 ROCK2 mediates effects of PCDH17 on actin organization and spine morphology

A: Representative images of immunostaining for phalloidin (Red) and Myc-PCDH17 (Green) in N2a cells. N2a cells were transfected with Myc-PCDH17 or control plasmids, treated with DMSO or KD025 (10 μmol/L) for 36 h, and stained at 48 h post-transfection. Scale bar: 10 μm. B, C: Quantitative analysis of Myc-PCDH17 signal intensity (B) and phalloidin signal intensity and area (C) from images in A. Projected Z-stack confocal images were analyzed using ImageJ. n=29–46 cells per group. D: RT-qPCR was conducted to verify ROCK2-siRNA interference efficiency. N2a cells were transfected with Myc-PCDH17 and ROCK2-siRNA, followed by RT-qPCR examination of ROCK2 gene expression. n=3 each group. E: Representative images of immunostaining for phalloidin (Red), ROCK2 (Blue), and Myc-PCDH17 (Green) in N2a cells. N2a cells were transfected with Myc-PCDH17 or control plasmids, and co-transfected with either Ctrl-siRNA or ROCK2-siRNA1. Scale bar: 10 μm. F: Quantitative analysis of phalloidin and ROCK2 signal intensity from images in E. Projected Z-stack confocal images were analyzed using ImageJ. n=21–30 cells per group. G, H: Immunoblotting analysis (G) and quantification (H) of ROCK2, cofilin, pCofilin and PCDH17 in N2a cells. n=3 per group. I: Representative images of LifeAct-mScarlet (Red) in cultured neurons. Scale bar: 10 μm. J: Quantitative analysis of LifeAct-mScarlet intensity in cultured neurons from I. n=20–22 neurons per group. K: Representative images of secondary dendrites from cultured neurons at DIV18. Neurons (DIV14) were transfected with Myc-PCDH17 or control plasmids along with an EGFP construct, then treated with DMSO or KD025 (10 μmol/L) for 48 h at 24 h post-transfection. Scale bar: 5 μm. L: Quantitative analysis of spine density at secondary dendrites in cultured neurons from D. n=14–33 neurons per group. Data are mean±SEM. ns: No significance; *: $P<0.05$; **: $P<0.01$; ***: $P<0.001$; ****: $P<0.0001$, One-way ANOVA and Dunn's test.

intensity and area, abolishing the F-actin defects caused by elevated PCDH17 levels (Figure 7A–C). For further inhibition, we designed and transfected two siRNAs targeting ROCK2

into N2a cells. Subsequent RT-qPCR analysis confirmed that siRNA1 effectively reduced ROCK2 expression (Figure 7D). We then transfected ROCK2 siRNA1 and control siRNA into

N2a cells along with the PCDH17 construct, followed by phalloidin staining 2 days later. Inhibition of ROCK2 expression with siRNA mitigated the reduction in phalloidin intensity in cells transfected with the PCDH17 construct (Figure 7E, F). Similarly, immunoblotting revealed that the increase in pCofilin (Ser3) levels in PCDH17-overexpressing N2a cells was restored by ROCK2 knockdown with siRNA transfection (Figure 7G, H). To determine the role of ROCK2 in mediating the effects of PCDH17 on actin cytoskeleton organization during synapse development, we transfected PCDH17 and control plasmid into cultured neurons (DIV14) along with the LifeAct-mScarlet construct, then applied KD025 for 48 h at 2 days post-transfection. Results showed that KD025 treatment alleviated the reduction in LifeAct-mScarlet intensity in PCDH17-transfected neurons (Figure 7I, J), demonstrating that ROCK2 mediates the effects of PCDH17 on F-actin organization.

We next determined whether PCDH17 modulates spine formation via ROCK2. Primary cultured neurons at DIV14 were transfected with PCDH17 and control vectors along with an EGFP construct, then treated with KD025 for 36 h at 3 days post-transfection. In DMSO-treated neurons, PCDH17 overexpression reduced spine density (Figure 7K, L, DMSO: 5.091±0.2755 total spines/10 µm in empty vector-transfected neurons, 4.043±0.2576 spines/10 µm in Myc-PCDH17-transfected neurons, P=0.0121; 2.74±0.1558 mushroom spines/10 µm in empty vector-transfected neurons, 1.923± 0.169 mushroom spines/10 µm in Myc-PCDH17-transfected neurons, P=0.0014; n=14-34), consistent with our previous results (Figures 1D, E; Supplementary Figure S1A–D). In PCDH17-transfected neurons, dendritic spine density, as well as that of mushroom and stubby spines, was significantly increased upon KD025 administration (Figure 7K, L, 4.043±0.2576 spines/10 µm in DMSO-treated PCDH17 neurons; 5.336±0.1986 spines/10 µm in KD025-treated PCDH17 neurons; P=0.0006; 1.923±0.169 mushroom spines/10 µm in DMSO-treated PCDH17 neurons, 2.698±0.1618 mushroom spines/10 µm in KD025-treated PCDH17 neurons, P=0.0157; n=14–34). Moreover, spine densities were comparable in KD025-treated PCDH17-overexpressing neurons and DMSO-treated control neurons (Figure 7K, L). Together, these results suggest that inhibition of ROCK2 rescues the spine defects induced by PCDH17 overexpression.

Pharmacological inhibition of ROCK2 with KD025 partially ameliorates anxiogenic and depression-like behavior caused by viral-mediated overexpression of PCDH17 in the vHPC

We next explored whether increased levels of ROCK2 contribute to the behavioral deficits caused by PCDH17 overexpression in the vHPC. Two-month-old C57BL/6J wild-type mice were injected with Lv-PCDH17 and Lv-Ctrl viruses in the vHPC and administered KD025 or vehicle for 3 days by oral gavage at 14 days post-injection. Subsequently, the mice were subjected to MBT, OFT, TST, and FST, which previously showed notable changes due to PCDH17 overexpression (Supplementary Figure S6A). In the MBT, the increased number of marbles buried by Lv-PCDH17-injected mice was markedly restored by KD025 treatment (Supplementary Figure S6B, C). In the OFT, KD025 treatment slightly increased the entry times and distance traveled in the center area by Lv-PCDH17-injected mice, although this did not reach statistical

significance (Supplementary Figure S6D, E). Furthermore, in the TST and FST, KD025 treatment partially abolished the increase in immobility time in PCDH17-overexpressing mice (Supplementary Figure S6F, G). Collectively, these findings suggest that pharmacological inhibition of ROCK2 can partially rescue the mood-related deficits observed in mice with PCDH17 overexpression.

DISCUSSION

This study showed that PCDH17 prevented the overgrowth of dendritic spines during postnatal development of neurons. Inhibition of PCDH17 expression during the critical period of synaptogenesis increased spine density. Increased abundance of PCDH17 inhibited the number of dendritic spines and restrained the size of mushroom spines during development and in adulthood via modulation of ROCK2-dependent F-actin organization. Moreover, viral-induced overexpression of PCDH17 in the vHPC resulted in anxiety- and depression-like behavior in mice, corroborating the involvement of increased PCDH17 in mood disorders.

Actin cytoskeletons are highly enriched at dendritic spines and play essential roles in modulating spine development and structural and functional remodeling (Dillon & Goda, 2005; Hotulainen & Hoogenraad, 2010). Here, we showed that PCDH17 interacted with actin-associated proteins and influenced F-actin content. Through AP-MS, we identified several actin-related proteins potentially associated with PCDH17 (Figure 4), among which ROCK2 was experimentally confirmed via colocalization and co-IP analyses (Figure 5). Furthermore, the impact of PCDH17 on F-actin organization was primarily mediated through ROCK2, as selective inhibition of ROCK2 activity abolished the influence of PCDH17 on F-actin content (Figure 7A–C). ROCKs, including ROCK1/2, are known to regulate actin-myosin-mediated cytoskeleton remodeling (Leung et al., 1995, 1996; Matsui et al., 1996), with ROCK2 preferentially acting through the LIMK1/cofilin pathway to regulate F-actin depolymerization and synapse number (Henderson et al., 2019; Peng et al., 2019). ROCK2 levels are positively correlated with cofilin Ser3 phosphorylation across various cellular contexts and diseases (Peng et al., 2019; Shi et al., 2013; Zhou et al., 2009). Our results indicated that overexpression of PCDH17 enhanced the protein levels of ROCK2, LIMK1, and pCofilin (Ser3), without altering their transcriptional levels. Hence, PCDH17 may stabilize the ROCK2-containing protein complex, triggering the activation of ROCK2-mediated downstream signaling. The ROCK2/LIMK1/pCofilin signaling cascade has been implicated in synapse loss associated with Alzheimer's disease (Henderson et al., 2019; Rush et al., 2018). Our findings provide novel insights into the pathogenic effects of ROCK2/LIMK1/pCofilin in synapse abnormalities related to mood disorders.

Our results further demonstrated that PCDH17 interacted with ROCK2 to regulate actin cytoskeleton organization and dendritic spine morphogenesis. Our MS analyses also indicated that PCDH17 may bind to other actin-related proteins. Previous research has reported that PCDH17 interacts with WAVE complex proteins to regulate axon extension (Hoshina et al., 2013). In addition, we observed that inhibition of ROCK2 with KD025 or siRNA transfection partially restored the decline in F-actin content induced by PCDH17 overexpression (Figure 7A, C, E, F). This suggests that PCDH17 may interact with actin or other actin-regulating

proteins during spine development. The influence of ROCK2 on spine development is complex and diverse in terms of neuronal type and spatial localization of dendrites (Swanger et al., 2015; Weber et al., 2021), and it also regulates the proportion of different types of dendritic spines (Weber et al., 2021). Further comprehensive investigations into the impact of PCDH17 on synapse development in different intact neuronal circuits *in vivo* are necessary. Genetic deletion of ROCK2 results in anxiety-like behavior in mice (Weber et al., 2021). In the present study, enhanced anxiety was correlated with increased expression of ROCK2 and activation of its downstream signaling, while inhibition of ROCK2 partially rescued the behavioral deficits caused by PCDH17 overexpression (Supplementary Figure S6), highlighting the complex role of ROCK2 signaling in behavioral regulation. The mechanism by which ROCK2 modulation affects behavioral performance may vary depending on its up- or down-regulation.

Moreover, in addition to its functions in the development of dendritic spines, the modification of actin dynamics is essential for the structural remodeling associated with various forms of synaptic plasticity (Yan et al., 2016). For instance, cofilin rapidly and persistently accumulates at synapses during long-term potentiation (Bosch et al., 2014), and cofilin-mediated actin dynamics facilitate AMPA receptor trafficking during long-term potentiation (Gu et al., 2010). Our observations that PCDH17 modulates cofilin phosphorylation imply that PCDH17 may also play a role in the regulation of certain types of synaptic plasticity, warranting further investigation.

Our findings also demonstrated that pharmacological inhibition of ROCK2 reversed the reduced spine density and spine area in PCDH17-overexpressing neurons (Figure 7K, L), suggesting that ROCK2 mediates the effects of PCDH17 on spine phenotype. Overexpression of ROCK2 has been shown to result in a reduction in spine number (Henderson et al., 2019). Moreover, inhibiting LIMK1 kinase activity, which reduces its effects on cofilin Ser3 phosphorylation, has been reported to alleviate ROCK2-induced spine loss (Henderson et al., 2019). Thus, elevated ROCK2 levels can restrict spine number through the LIMK1/pCofilin signaling pathway. In our study, increased abundance of LIMK1 and elevated cofilin Ser3 phosphorylation were detected in the PCDH17-overexpressing neurons and N2a cells. These findings indicate that PCDH17 may bind to ROCK2, thereby activating its downstream signaling targets LIMK1/pCofilin to modulate spine number and morphology. However, ROCK2 has many other substrates (Amano et al., 2015), and the potential contributions of other downstream signaling pathways of ROCK2 in PCDH17-regulated F-actin organization and synapse structure cannot be excluded.

Genetic analyses have linked PCDH17 to major mood disorders, such as bipolar disorder and depression (Chang et al., 2018). However, the neurobiological mechanisms through which PCDH17 mutations influence these mood disorders remain unclear. Our results indicated that increased expression of PCDH17 led to heightened anxiety and depressive behaviors in mice, in accordance with increased expression of PCDH17 in patients with major mood disorders (Chang et al., 2018). In addition, we discovered that disturbances in the ROCK2-mediated actin cytoskeleton may underpin the spine dysregulation induced by PCDH17 overexpression. Emerging evidence has suggested that

synaptic abnormalities and actin disruptions play critical roles in the pathology of many mental illnesses (Parekh et al., 2022; Penzes et al., 2011; Yan et al., 2016). Synaptogenesis is considered an important biological basis for mood state transitions in depression (Parekh et al., 2022). Hence, our findings suggest that the spine density and morphological alterations induced by PCDH17 may be instrumental in its effects on affective responses, providing mechanistic insights into the role of PCDH17 in mood disorders.

LIMITATIONS OF THE STUDY

In this study, we revealed that PCDH17 increased the protein level of ROCK2 without impacting its mRNA level, suggesting that PCDH17 may stabilize ROCK2 by forming a complex with it and its downstream effectors, such as LIMK1 and pCofilin. However, further research is needed to confirm this possibility. We also employed a lentivirus-mediated strategy to overexpress PCDH17 in excitatory neurons in mice using a CaMK2α promoter. Given the potential non-specific effects of gene overexpression and the non-specificity of viral infection, PCDH17 knock-in using the Cre-lox system will be utilized in the future to further clarify the role of PCDH17 in synapse development and animal behavior.

SUPPLEMENTARY DATA

Supplementary data to this article can be found online.

COMPETING INTERESTS

The authors declare that they have no competing interests.

AUTHORS' CONTRIBUTIONS

REFERENCES

Alvarez VA, Sabatini BL. 2007. Anatomical and physiological plasticity of dendritic spines. *Annual Review of Neuroscience*, **30**: 79–97.

Amano M, Hamaguchi T, Shohag H, et al. 2015. Kinase-interacting substrate screening is a novel method to identify kinase substrates. *Journal of Cell Biology*, **209**(6): 895–912.

Berry KP, Nedivi E. 2017. Spine dynamics: are they all the same?. *Neuron*, **96**(1): 43–55.

Bosch M, Castro J, Saneyoshi T, et al. 2014. Structural and molecular remodeling of dendritic spine substructures during long-term potentiation. *Neuron*, **82**(2): 444–459.

Chang H, Hoshina N, Zhang C, et al. 2018. The protocadherin 17 gene affects cognition, personality, amygdala structure and function, synapse development and risk of major mood disorders. *Molecular Psychiatry*, **23**(2): 400–412.

Dillon C, Goda Y. 2005. The actin cytoskeleton: integrating form and function at the synapse. *Annual Review of Neuroscience*, **28**: 25–55.

Forrest MP, Parnell E, Penzes P. 2018. Dendritic structural plasticity and neuropsychiatric disease. *Nature Reviews Neuroscience*, **19**(4): 215–234.

Gao QT, Tian RY, Han HL, et al. 2022. PINK1-mediated Drp1^{S616} phosphorylation modulates synaptic development and plasticity via

promoting mitochondrial fission. *Signal Transduction and Targeted Therapy*, **7**(1): 103.

Gu JP, Lee CW, Fan YJ, et al. 2010. ADF/cofilin-mediated actin dynamics regulate AMPA receptor trafficking during synaptic plasticity. *Nature Neuroscience*, **13**(10): 1208–1215.

Hayashi S, Inoue Y, Kiyonari H, et al. 2016. Protocadherin-17 mediates collective axon extension by recruiting actin regulator complexes to interaxonal contacts. *Developmental Cell*, **38**(3): 331.

Henderson BW, Greathouse KM, Ramdas R, et al. 2019. Pharmacologic inhibition of LIMK1 provides dendritic spine resilience against β-amyloid. *Science Signaling*, **12**(587): eaaw9318.

Hoshina N, Tanimura A, Yamasaki M, et al. 2013. Protocadherin 17 regulates presynaptic assembly in topographic corticobasal Ganglia circuits. *Neuron*, **78**(5): 839–854.

Hotulainen P, Hoogenraad CC. 2010. Actin in dendritic spines: connecting dynamics to function. *Journal of Cell Biology*, **189**(4): 619–629.

Hu ZH, Yu DN, Gu QH, et al. 2014. miR-191 and miR-135 are required for long-lasting spine remodelling associated with synaptic long-term depression. *Nature Communications*, **5**: 3263.

Kedia S, Chattarji S. 2014. Marble burying as a test of the delayed anxiogenic effects of acute immobilisation stress in mice. *Journal of Neuroscience Methods*, **233**: 150–154.

Kim SY, Mo JW, Han S, et al. 2010. The expression of non-clustered protocadherins in adult rat hippocampal formation and the connecting brain regions. *Neuroscience*, **170**(1): 189–199.

Lee JH, Zheng Y, von Bornstadt D, et al. 2014. Selective ROCK2 inhibition in focal cerebral ischemia. *Annals of Clinical and Translational Neurology*, **1**(1): 2–14.

Leung T, Chen XQ, Manser E, et al. 1996. The p160 RhoA-binding kinase ROKα is a member of a kinase family and is involved in the reorganization of the cytoskeleton. *Molecular and Cellular Biology*, **16**(10): 5313–5327.

Leung T, Manser E, Tan L, et al. 1995. A novel serine/threonine kinase binding the ras-related RhoA GTPase which translocates the kinase to peripheral membranes. *Journal of Biological Chemistry*, **270**(49): 29051–29054.

Li J, Zhang WS, Yang H, et al. 2017. Spatiotemporal profile of postsynaptic interactomes integrates components of complex brain disorders. *Nature Neuroscience*, **20**(8): 1150–1161.

Liao PL, Yuan YC, Liu Z, et al. 2022. Association of variants in the *KIF1A* gene with amyotrophic lateral sclerosis. *Translational Neurodegeneration*, **11**(1): 46.

Lin YC, Koleske AJ. 2010. Mechanisms of synapse and dendrite maintenance and their disruption in psychiatric and neurodegenerative disorders. *Annual Review of Neuroscience*, **33**: 349–378.

Liu MY, Yin CY, Zhu LJ, et al. 2018. Sucrose preference test for measurement of stress-induced anhedonia in mice. *Nature Protocols*, **13**(7): 1686–1698.

Maekawa M, Ishizaki T, Boku S, et al. 1999. Signaling from Rho to the actin cytoskeleton through protein kinases ROCK and LIM-kinase. *Science*, **285**(5429): 895–898.

Matsui T, Amano M, Yamamoto T, et al. 1996. Rho-associated kinase, a novel serine/threonine kinase, as a putative target for small GTP binding protein Rho. *The EMBO Journal*, **15**(9): 2208–2216.

Njung'e K, Handley SL. 1991. Effects of 5-HT uptake inhibitors, agonists and antagonists on the burying of harmless objects by mice; a putative test for anxiolytic agents. *British Journal of Pharmacology*, **104**(1): 105–112.

Parekh PK, Johnson SB, Liston C. 2022. Synaptic mechanisms regulating mood state transitions in depression. *Annual Review of Neuroscience*, **45**: 581–601.

Parisiadou L, Yu J, Sgobio C, et al. 2014. LRRK2 regulates synaptogenesis and dopamine receptor activation through modulation of PKA activity. *Nature Neuroscience*, **17**(3): 367–376.

Peng YT, Chen ZY, Chen Y, et al. 2019. ROCK isoforms differentially modulate cancer cell motility by mechanosensing the substrate stiffness. *Acta Biomaterialia*, **88**: 86–101.

Penzes P, Cahill ME, Jones KA, et al. 2011. Dendritic spine pathology in neuropsychiatric disorders. *Nature Neuroscience*, **14**(3): 285–293.

Reimand J, Isserlin R, Voisin V, et al. 2019. Pathway enrichment analysis and visualization of omics data using g: profiler, GSEA, Cytoscape and EnrichmentMap. *Nature Protocols*, **14**(2): 482–517.

Riedl J, Crevenna AH, Kessenbrock K, et al. 2008. Lifeact: a versatile marker to visualize F-actin. *Nature Methods*, **5**(7): 605–607.

Rush T, Martinez-Hernandez J, Dollmeyer M, et al. 2018. Synaptotoxicity in alzheimer's disease involved a dysregulation of actin cytoskeleton dynamics through cofilin 1 phosphorylation. *The Journal of Neuroscience*, **38**(48): 10349–10361.

Shi JJ, Wu XB, Surma M, et al. 2013. Distinct roles for ROCK1 and ROCK2 in the regulation of cell detachment. *Cell Death & Disease*, **4**(2): e483.

Stucchi R, Plucińska G, Hummel JJA, et al. 2018. Regulation of KIF1A-driven dense core vesicle transport: Ca^{2+}/CaM controls DCV binding and liprin-α/TANC2 recruits DCVs to postsynaptic sites. *Cell Reports*, **24**(3): 685–700.

Südhof TC. 2018. Towards an understanding of synapse formation. *Neuron*, **100**(2): 276–293.

Swanger SA, Mattheyses AL, Gentry EG, et al. 2015. ROCK1 and ROCK2 inhibition alters dendritic spine morphology in hippocampal neurons. *Cellular Logistics*, **5**(4): e1133266.

Tada T, Sheng M. 2006. Molecular mechanisms of dendritic spine morphogenesis. *Current Opinion in Neurobiology*, **16**(1): 95–101.

Ting JT, Peça J, Feng GP. 2012. Functional consequences of mutations in postsynaptic scaffolding proteins and relevance to psychiatric disorders. *Annual Review of Neuroscience*, **35**: 49–71.

Trubetskoy V, Pardiñas AF, Qi T, et al. 2022. Mapping genomic loci implicates genes and synaptic biology in schizophrenia. *Nature*, **604**(7906): 502–508.

Wang T, Zhou YQ, Wang Y, et al. 2023. Long-term potentiation-based screening identifies neuronal PYGM as a synaptic plasticity regulator participating in Alzheimer's disease. *Zoological Research*, **44**(5): 867–881.

Weber AJ, Adamson AB, Greathouse KM, et al. 2021. Conditional deletion of ROCK2 induces anxiety-like behaviors and alters dendritic spine density and morphology on CA1 pyramidal neurons. *Molecular Brain*, **14**(1): 169.

Yan Z, Kim E, Datta D, et al. 2016. Synaptic actin dysregulation, a convergent mechanism of mental disorders?. *Journal of Neuroscience*, **36**(45): 11411–11417.

Zhou ZK, Meng YH, Asrar S, et al. 2009. A critical role of Rho-kinase ROCK2 in the regulation of spine and synaptic function. *Neuropharmacology*, **56**(1): 81–89.